ApJ, in press
Preprint typeset using LaTeX style emulateapj v. 08/13/06

arXiv:1408.5473v1 [astro-ph.SR] 23 Aug 2014

MEASUREMENTS OF OUTFLOW VELOCITIES IN ON-DISK PLUMES FROM EIS/HINODE OBSERVATIONS

Hui Fu[1], Lidong Xia[1*], Bo Li[1], Zhenghua Huang[1], Fangran Jiao[1], Chaozhou Mou[1]

Draft version August 26, 2014

ABSTRACT

The contribution of plumes to the solar wind has been subject to hot debate in the past decades. The EUV Imaging Spectrometer (EIS) on board Hinode provides a unique means to deduce outflow velocities at coronal heights via direct Doppler shift measurements of coronal emission lines. Such direct Doppler shift measurements were not possible with previous spectrometers. We measure the outflow velocity at coronal heights in several on-disk long-duration plumes, which are located in coronal holes and show significant blue shifts throughout the entire observational period. In one case, a plume is measured 4 hours apart. The deduced outflow velocities are consistent, suggesting that the flows are quasi-steady. Furthermore, we provide an outflow velocity profile along the plumes, finding that the velocity corrected for the line-of-sight effect can reach 10 $\mathrm{km\,s^{-1}}$ at 1.02 $R_\odot$, 15 $\mathrm{km\,s^{-1}}$ at 1.03 $R_\odot$, and 25 $\mathrm{km\,s^{-1}}$ at 1.05 $R_\odot$. This clear signature of steady acceleration, combined with the fact that there is no significant blue shift at the base of plumes, provides an important constraint on plume models. At the height of 1.03 $R_\odot$, EIS also deduced a density of 1.3×10^8 $\mathrm{cm^{-3}}$, resulting in a proton flux of about 4.2×10^9 $\mathrm{cm^{-2}s^{-1}}$ scaled to 1AU, which is an order of magnitude higher than the proton input to a typical solar wind if a radial expansion is assumed. This suggests that, coronal hole plumes may be an important source of the solar wind.

Subject headings: Sun: plume — Sun: Doppler shift — Sun: solar wind — EUV

1. INTRODUCTION

Solar plumes are ray-like bright structures extending from the base of the corona into the high corona (DeForest et al. 2001b; see also Wilhelm et al. 2011 for a recent review). They are the most conspicuous structures observed during a total eclipse (Van de Hulst 1950a,b). They can be observed in both visible light and EUV (Wilhelm et al. 2011, and references therein). By tracing plume structures up to 15 $R_\odot$, DeForest et al. (1997, 2001a) have demonstrated that the structures seen in visible light and EUV are different parts of the same phenomenon. Plumes are found to be rooted mainly at mid- and high-latitudes where the global magnetic fields are open into interplanetary space. Regarding magnetic field at their foot-points, many people believe that plumes are associated with mixed-polarity magnetic features with small bipolar fields interacting with background unipolar fields (Wang & Sheeley 1995; Wang & Muglach 2008). So far, most studies on plumes are carried out in and above polar coronal holes (PCHs) thanks to the faint background that makes plumes easy to be observed. However, some efforts have also been made to study the properties of plumes at lower latitudes seen in EUV (Wang & Sheeley 1995; Zanna & Bromage 1999; Zanna et al. 2003; Wang & Muglach 2008; Tian et al. 2011), white light (Yang et al. 2011) and radio wavelengths (Woo 1996). These studies have demonstrated the existence of plumes at lower latitudes and have shown that the properties of mid- and low-latitude plumes are similar to those of polar plumes (Zanna et al. 2003; Wang & Muglach 2008; Tian et al. 2011; Yang et al. 2011).

Coronal holes (CHs) are well believed to be the source regions of the fast solar wind (Krieger et al. 1973; Zirker 1977; Gosling & Pizzo 1999; Hassler et al. 1999; Xia et al. 2003a). Krieger et al. (1973) were the first to associate a fast stream with a coronal hole, while Zirker (1977) suggested that all coronal holes are connected to the fast solar wind. Since plumes are mainly found in CHs, their relationship with the solar wind became a significant problem. Using the photometric data obtained in the wavelength range between 171 Å and 175 Å combined with a simple, semi-empirical model of the solar wind, Walker et al. (1993) suggested that plumes are a possible source region of the solar wind. By using the Doppler Dimming technique, Gabriel et al. (2003, 2005) concluded that plumes could provide about half of the mass that the solar wind carries into interplanetary space. More recently, using high resolution AIA/SDO observations, McIntosh et al. (2010) and Tian et al. (2011) suggested that the high speed structures in plumes could provide mass flux to the solar wind efficiently. Nevertheless, the conclusion is still under debate. For instance, many studies showed no clear evidence that plumes could provide sufficient momentum and mass to solar wind flows (Wang 1994; Habbal et al. 1995; Wilhelm et al. 2000; Hassler et al. 1999; Giordano et al. 2000; Patsourakos & Vial 2000; Teriaca et al. 2003) .

The primary reason for ruling out plumes as a solar wind source is that the calculated mass flux in plumes is lower than needed by a typical solar wind. Evidently, such a calculation requires that the electron density and flow velocity be measured in plumes. Habbal et al. (1995) calculated the electron density in both plume and inter-plume regions in a PCH using the polarized white-light observations. Combining with a two-fluid model, they obtained the velocity in plume and inter-plume regions at different altitudes, and found that the velocity of the inter-plume region was faster than that of the plume re-

[1] Shandong Provincial Key Laboratory of Optical Astronomy and Solar-Terrestrial Environment, School of Space Science and Physics, Shandong University, Weihai 264209, China
[*] xld@sdu.edu.cn

gion. Through analyzing the O VI spectral data recorded by SUMER/SOHO, Wilhelm et al. (1998) measured the velocity in plumes below 1.2 $R_\odot$, and found that the outflow velocity was smaller than 18 $\mathrm{km\,s^{-1}}$ after the line-of-sight (LOS) projection was taken into account. In the same study, they also measured the velocity in inter-plume regions with the Mg IX line, and found that the LOS velocity was up to 34 $\mathrm{km\,s^{-1}}$. Therefore, they argue that the inter-plume lanes are the genuine source regions of the fast solar wind. Through analyzing two images simultaneously taken by the two EUVI telescopes on STEREO-A and -B, Feng et al. (2009) reconstructed the location and inclination of polar plumes. Then, the outflow velocity corrected for the LOS effect is as small as 10 $\mathrm{km\,s^{-1}}$ seen in O VI observed by SUMER. They concluded that the plumes are unlikely a main source of the fast solar wind when assuming a filling factor of plumes to be 0.1 in CHs (Ahmad & Withbore 1977). Tracing the dynamic features from 1.1 $R_\odot$ to 1.3 $R_\odot$ in white light observations during the total eclipse, Bĕlík et al. (2013) obtained a propagation speed ranging from 32 $\mathrm{km\,s^{-1}}$ to 146 $\mathrm{km\,s^{-1}}$, with an average value of 67 $\mathrm{km\,s^{-1}}$ in plume structures.

The Doppler Dimming technique (Rompolt 1967) is often used to derive the outflow velocity of off-limb plumes. In order to investigate how outflow velocities change with height at altitudes below 2 $R_\odot$, Teriaca et al. (2003) explored observations with SUMER/SOHO and UVCS/SOHO in a PCH, and from their results, they concluded that plumes are more or less static, so inter-plume regions are suggested as sources of the fast wind. In contrast, Corti et al. (1997) found that in the heliocentric range between 1.5 and 2.3 $R_\odot$, the outflow velocity in plumes is about the same as that in inter-plume regions. Using the same method, Gabriel et al. (2003, 2005) derived an even faster outflow velocity in plumes than in inter-plume regions below 1.6 $R_\odot$. Nevertheless, one word of caution is that the Doppler dimming method strongly depends on empirical assumptions of the electron density and ion temperature, thus may lead to different results with different assumptions (Wilhelm et al. 2011).

Obviously, measuring the Doppler shift on the disk is a more straightforward way of getting the outflow velocity in plumes. Some spectroscopic studies have been made for on-disk plumes. By analyzing the Ne VIII 770 Å line observed in a north PCH with SUMER, some authors (Hassler et al. 1999; Hassler 2000; Wilhelm et al. 2000) found that the base of the plumes does not show a clear blue shift compared to other CH regions. However, the above studies are based on observations with SUMER, which has limited spectral lines at coronal temperatures, so the measured radiation is mainly emitted by the bright cores at the bottom of plumes.

In this study, we use spectroscopic observations with the EUV Imaging Spectrometer (EIS) (Culhane et al. 2007) on board the Hinode satellite (Kosugi et al. 2007), which includes many coronal lines and covers a wide temperature range. It gives us an opportunity to study the Doppler velocities in the extended structure of plumes. Meanwhile, the influence of background is lower when the extended structure of plumes projects on the dark background of CHs. This offers a bigger advantage in observing plumes than SUMER does. The paper is organized as follows. In Section 2, we describe the observations and data analysis methods. The results are shown in Section 3. The significance of our results associated with the origin of the solar wind is discussed in Section 4. A conclusion is presented in Section 5.

2. OBSERVATION AND DATA ANALYSIS

Four data sets obtained by EIS are used in the present study. Among them, one data set was recorded in a mid-latitude region, the others were recorded in the north pole. Because we are interested in plumes that project on CHs, the data sets with long-exposure time and 2″ wide slit are chosen in order to have a good signal-to-noise ratio. The details of the scanning period, observed location, size of field of view (FOV) and exposure time for the selected data sets are listed in Table 1. In Table 2, we list eight lines with formation temperatures ranging from 50000 K to 2 million K (MK) that are used for analyzing the intensity contrast of plumes and the CH background. Among them, five lines with good signal-to-noise ratio and no obvious blends are chosen to deduce the Doppler shift. According to Young et al. (2007) and Tian et al. (2010), these lines can be well fitted by a single Gaussian. It is noteworthy that the data taken in 2007 have been used by Banerjee et al. (2009) to search for signatures of Alfvén waves and Tian et al. (2010) to describe the scenario of the nascent fast solar wind guided by expanding magnetic funnels. The difference between the study of Tian et al. (2010) and our work will be further discussed in Section 3. We also use the data from EIT on board SOHO, and AIA on board SDO to identify plumes.

The EIS data are calibrated by standard procedures including dark-current, flat-field, removal of cosmic rays, hot and warm pixels, and radiometric calibration via the routine *eis_prep.pro* provided by the instrumental team. EIS has two CCDs that cover the wavelengths from 170 Å to 210 Å and 250 Å to 290 Å respectively. Images taken by the two CCDs have offsets along the slit direction and raster-scanning direction due to the arrangement of the CCDs. According to our study, an offset of 16″ was found between the two CCDs along the slit direction, which is in agreement with the results found by Tian et al. (2010) and Démoulin et al. (2013). The procedure *eis_wave_corr.pro* in Solar software (SSW) is used to compensate for the orbital variations of the EIS line centers (Kamio et al. 2010) and the slit tilt caused by tilt of slits relative to the axes of the EIS CCDs.

Wavelength calibration is an important step for obtaining precise Doppler shifts of spectral lines. Unfortunately, EIS has neither absolute wavelength calibration on board nor cold lines as reference. However, there are two methods for obtaining the absolute Doppler shift, one assuming that the LOS velocity of the off-limb plasma is zero (Peter & Judge 1999; Kamio et al. 2007), the other assuming that the quiet-Sun (QS) region is almost quiet and can be used as a reference. The data set taken in 2007 includes both off-limb and QS observations, which provides an opportunity to verify the two methods. Because only Fe X 184.54 Å, Fe XII 195.12 Å and Fe XIII 202.04 Å have reliable signal-to-noise ratio in the off-limb data, we use them to derive the required referent wavelengths. We first obtain a spectrum by averaging all the spectra from 65″ to 143″ above the limb (Tian et al.

2010). By assuming that the average off-limb spectrum is zero-shifted, we then calculate the line shifts of an average spectrum of a QS region, where the Doppler velocities are found to be -3.0±2.8 $\mathrm{km\,s^{-1}}$, -3.3±2.8 $\mathrm{km\,s^{-1}}$, -3.9±2.8 $\mathrm{km\,s^{-1}}$ (here only fitting errors are considered) in Fe X 184.54 Å, Fe XII 195.12 Å and Fe XIII 202.04 Å, respectively, which are consistent with the results found by Peter & Judge (1999) and Dadashi et al. (2011). By using cospatial and nearly cotemporal SUMER and EIS data, Dadashi et al. (2011) obtained blue shifts (upward motions) between -2 to -4 $\mathrm{km\,s^{-1}}$ at temperatures between 1 and 1.8 MK. Therefore, we select the line center position averaged over a QS region, where a blue shift of 3.5 $\mathrm{km\,s^{-1}}$ is assumed, as the reference to calculate the absolute velocities of plumes in CHs.

An error analysis is necessary but not straightforward. Three components of errors contribute to the total error of the derived Doppler velocities: 1) the fitting error $\sigma_{\mathrm{fitting}}$, 2) the error associated with assigning an absolute speed (-3.5 $\mathrm{km\,s^{-1}}$ in this paper) to the QS region σ_{abs}, and 3) the error associated with the unphysical noisy stripes of the derived Dopplergrams σ_{noise}. It turns out that $\sigma_{\mathrm{fitting}}$ is the smallest among the three (varying between 0.1 and 0.2 $\mathrm{km\,s^{-1}}$), for the spectra employed as the input to the fitting procedure are obtained by averaging the relevant spectra over a substantial area and therefore are close to a perfect Gaussian. As for σ_{abs}, Dadashi et al. (2011) established that for spectral lines with formation temperatures between 1 and 1.8 MK, this error ranges from 2.0 to 3.0 $\mathrm{km\,s^{-1}}$ (see their Table 3), here the median value of 2.2 $\mathrm{km\,s^{-1}}$ is chosen for our purpose. σ_{noise} can be estimated by computing the standard deviation of the derived Dopplergrams over a selected area with visible vertical and/or horizontal artifacts. For dataset 1, the off limb region is chosen whereby σ_{noise} is estimated to be 1.7 $\mathrm{km\,s^{-1}}$. However, for datasets 2, 3, 4, the Dopplergrams are not as well organized as the one for dataset 1 (compare Figures 5(b), 7(b1), 7(b2) with Figure 3(d2)): some horizontal and vertical stripes show up in e.g., the middle part in the lower half of Figures 5(b) and 7(b2)), their origin likely to be unphysical. Therefore we compute σ_{noise} in the regions where these artifacts are most evident in order not to underestimate this error, finding that σ_{noise} reads 1.8 (2.1, 3.3) $\mathrm{km\,s^{-1}}$ in dataset 2 (3, 4). We then evaluate the desired total error σ according to $\sigma = \sqrt{\sigma_{\mathrm{fitting}}^2 + \sigma_{\mathrm{abs}}^2 + \sigma_{\mathrm{noise}}^2}$, the results being 2.8, 2.8, 3.0, and 4.0 $\mathrm{km\,s^{-1}}$ for datasets 1 to 4, respectively.

The identification of plumes in on-disk images is not straightforward. To make plumes easier to identify, a method called Multi-scale Gaussian Normalization (MGN) (Morgan & Druckmüller 2014) is applied. This method helps reveal fine scales without the loss of larger-scale information.

3. RESULTS

In Figure 1, we show the intensity map (middle panel) derived from the EIS raster scan in Fe XIII 202.04 Å on 2007 October 10, together with the corresponding EIT 195 Å image (left panel) with a larger field of view (FOV) and processed image of intensity map using the method MGN. As previous studies have demonstrated, plumes are identified as faint and diffuse blobs of emission-enhanced structure with a brighter core seen in EUV on the disk (Wang & Muglach 2008). Accordingly, we may identify a number of plumes in this data set. Among them three plumes outlined by the green solid lines (labeled PL1, PL2 and PL3) have clearly extended structures in the EIS FOV by an inspection of the corresponding processed image. The three plumes are extending to heights of around 80 to 100 arcsec, which are further divided into three sub-regions as bottom, middle, and top segments marked by the white rectangles for further analysis. Please note that plumes are not clearly seen in the EIT image, perhaps due to the lower sensitivity of EIT relative to EIS. Using the same procedures, we also identify and select three plumes in the other three data sets for analysis.

In CH plumes, the measured emission mainly comprises two components: the plumes themselves and CH background. In order to estimate their specific contribution, here we define a parameter called the *relative radiation intensity* (*RRI=intensity of selected region/mean QS intensity*). *RRI* represents the intensity ratio of a selected region and the mean QS region. Fortunately, the EIS FOVs cover QS regions in every event.

In Figure 2, we display the *RRI* parameter of three plumes measured in the spectral lines of interest recorded on 2007 October 10. For comparison, the *RRI* measurement of a typical dark region as seen in hot coronal lines in the CH is also presented. From Figure 2, one finds that the intensity of He II is generally weaker in the entire CH region including plumes than in the QS region, which is consistent with the previous EIT observations. For the dark CH region, the *RRI* has a value larger than 1 in both Fe VIII and Si XII lines with formation temperatures below 1 MK. This may be caused by the existence of the underlying bright network structures (also see Figure 3). The *RRI* decreases quickly to 0.2 in Fe X. This is a typical result observed previously by SUMER (Xia 2003b). However, for the coronal lines whose formation temperatures exceed 1 MK, the *RRI*s of the dark CH region are all less than 0.1 and nearly constant (0.09, 0.08, 0.08 in Fe XII 195.12 Å, Fe XIII 202.04 Å and Fe XV 284.16 Å, respectively). This is very likely caused by the stray light and the reason why we can only obtain smaller blue shifts from these three lines in the dark region, which are comparable with those obtained in the QS region (see further discussion below).

For plumes, the *RRI* reaches maximum in the extended structure for Fe VIII and Si XII lines, which can be larger or smaller than 1. These lines seem to be mainly emitted by the network structures underlying the extended structure of plumes. Nevertheless, the *RRI* reaches a minimum for the Fe XII and Fe XIII lines and then increases again with formation temperature. Moreover, line intensities of Fe XII, Fe XIII, Fe XV are much stronger than those of the CH background as shown in Figure 2. Quantitatively, this may be illustrated by examining the specific *RRI* values. Take the plume PL3, the weakest in emission among the three plumes, for instance. For its top segment, the *RRI* reads 0.26 in Fe XII, 0.30 in Fe XIII, and 0.34 in Fe XV. As a comparision, the background coronal hole corresponds to *RRI* values of 0.09, 0.08, and 0.08 for the three passbands, respectively. Consequently, the contribution of the plume plasma to the

overall emission can be estimated to be 65% in Fe XII, 73% in Fe XIII, and 76% in Fe XV. Given that the top segments are subject to a stronger contamination from the emission from the background coronal hole, and that the plume PL3 suffers from the strongest contamination among the three plumes, we then deduce that in Fe XII (Fe XIII, Fe XV), at least 65% (73%, 76%) of the emission comes from the plume plasma itself. Actually, the derived relative contribution is consistent with those obtained by Tian et al. (2011).

Given that the plumes were deduced to be less hot than inter-plume regions (DeForest et al. 1997; Hassler et al. 1997; Banerjee et al. 2000), one may question why they emit in a line as hot as Fe XV as well. Raouafi et al. (2008) find plumes are associated with hot and transit X-ray jets, and the lifetimes of those jets range from minutes to a few tens of minutes. It then follows that the plumes we examine may be also associated with X-ray emitting, hot structures as well. However, a close examination indicates that the main structures of plumes are almost quasi-steady. The plumes in data sets 2 to 4 have lifespans exceeding 4 hours, and their morphology remains stable in the time interval we examined (see the AIA movies and running difference movies: movie20100904, movie20100904diff, movie20110111 and movie20110111diff in the supplement). In AIA movies (especially for data set 20110111), like Raouafi et al. (2008) found, there are many small transient structures at the base of plumes. Those explosive events are smaller in size (only several arcsecs) and weaker in intensity (the intensity changes by no more than 10%) compared to quasi-steady plume structures. For comparison, there is a classic jet in AIA movie20100904 (t=00:10-00:25, x=-75″, y=900″) for which the intensity increased by 35% in the 171 band, and by 50% in the 193 band when the jet erupts. We suspect that the major plume plasmas can be supplied by those small transient events. As for the plumes in data set 1 acquired in 2007, the EIT 195 movie suggests that they are stable and not associated with big explosive events. One then naturally ask whether stable plumes also emit in hot lines. Actually, DeForest et al. (1997) also noticed that plumes are seen not only in EIT 171 movie and EIT 195 images, but also in the Fe XV 284 band. One possibility is that, although the temperature of plumes is lower than in inter-plume regions, but plumes themselves may contribute to a significant fraction of the corresponding emission due to their considerably higher densities than the surrounding coronal hole plasmas. Another possibility that cannot be ruled out is that the plume structures are composed of hot subresolution transients. Not resolved adequately in current observations, these transients may make the plume structures appear quasi-stable.

The intensity and Dopplergram maps derived from the Fe VIII, Si VII, Fe X, Fe XII and Fe XIII lines are displayed in Figure 3. Figure 3 brings to our attention that the strong blue-shift patches derived from hot lines of Fe X, Fe XII and Fe XIII coincide with the extended structures of the identified plumes. In contrast, this coincidence is not clear in cooler lines of Fe VIII and Si VII, where the intensity and Dopper-shift patterns reflect mainly local network structures but not plumes. As we have mentioned, there are smaller blue shifts in the dark region of the CH, which is contoured by white lines in Figure 1 (middle panel) and red lines in Figure 3. The Doppler shift is -2.4 $\mathrm{km\,s^{-1}}$ in Fe XII 195.12 Å and -3.4 $\mathrm{km\,s^{-1}}$ in Fe XIII 202.04 Å respectively, which is comparable with the QS region. Combining with the fact that in the region where plume structure projects on the CH background the radiation is mainly from plume structure for those lines with formation temperatures in excess of 1 MK, we can draw an important conclusion that the Doppler shift in the region where plume structure projects on CH reflects the outflow in plume structures.

The above analysis has further demonstrated our identification of the extended structure of plumes, which differs from the explanation of Tian et al. (2010), where they interpreted the blue-shift patches in Figure 3 as evidence of the nascent fast solar wind originating from the underlying magnetic networks. In a later paper, Tian et al. (2011) have also clarified that in this data set the blue-shift patches in CH are mainly contaminated by the plumes rooted at the boundary of the PCH (see Figure 8 in their paper).

Figure 4 shows the outflow velocity along the plumes derived from the Fe VIII, Si VII, Fe X, Fe XII and Fe XIII lines. At first glance, it is a little strange that the Doppler shifts seen in the very hot lines are much different from those in colder lines at the same height. Then, which ones reflect the real Doppler shifts of plume structures? Here we argue that the Doppler shifts of the hottest lines whose formation temperatures exceed 1 MK reflect more faithfully the real outflow in plumes. As shown in Figure 3(a1) and 3(b1), the plume structures are almost invisible in the lines of Fe VIII and Si VII, which means that the emission from the CH background dominates in these cool lines. This may be further corroborated by Figures 3(a2) and 3(b2), where the Dopplergrams are shown. In contrast to the Doppler shift features in hot lines (Figures 3(c2-e2)), the Doppler features are not organized in linear shapes as seen in the intensity diagrams. In practice, we derive our outflow speeds for plumes using only the Fe XIII line. The reason we do not use the hottest line, Fe XV, is that the spectral shape is not as good as the Fe XIII line. In this way, we can draw a further conclusion that Doppler shifts increase with height in the extended structure of plumes. Furthermore, assuming that the plumes are extending radially, one can deduce the outflow velocity of the plume plasma by correcting the latitude/LOS effect of the plumes. For plumes of the 2007 October 10 data set, the latitude of the plumes is about 60 degree. The outflow velocity derived from the hottest line increases with height in the plumes, and reads about 10 ± 5.6 $\mathrm{km\,s^{-1}}$ at 1.02 $R_\odot$, 15 ± 5.6 $\mathrm{km\,s^{-1}}$ at 1.03 $R_\odot$, and 25 ± 5.6 $\mathrm{km\,s^{-1}}$ at 1.05 $R_\odot$.

If a plume is observed near the equator and its orientation is nearly parallel to the local radial direction, it will allow us to derive its outflow velocity directly from Doppler shifts with a less strong projection effect. Fortunately, we observed a low latitude plume in the data set of 2011 Jan 11 as show in Figure 5. The plume (marked by the ellipse) is located at the boundary of a big low latitude CH. Although it is not very clearly seen in the EIS Fe XII 195.12 Å intensity map, it can be easily identified in the AIA 171 Å movie. The Doppler shifts of the plume structure and CH region (marked by the rectangle) are shown in Figure 6. Green, blue and red curves represent

the Doppler shifts of QS, CH and plume regions, respectively. We find the Doppler shift of plume structure is larger than 20 km s^{-1} in the coronal line Fe XII 195.12 Å, which is consistent with the corrected velocity derived from the 2007 Oct 10 event.

A question may arise as to whether these blue-shift patches are quasi-steady outflows or velocity patterns associated with transient events. This is necessary given that DeForest et al. (2001a) and Raouafi et al. (2008) have shown that plumes appear to be recurrent and bursty. To address this question, we follow a plume imaged by four hours apart on 2010 Sep 4, which are shown in Figure 7. The top panels show the intensity and Dopplergram observed from 18:30 to 22:02, and the bottom panels are for the measurements between 22:04 and 01:36 the following day. Among several plume structures, one projected on CH and marked by the white rectangle is chosen for further analysis. From Figure 7, the shape of the plume does not change substantially in the two scans. Now the question is whether the plumes may have pulsed twice? We then examined the AIA movie for the corresponding time interval (movie20100904, now supplemented to Figure 7), and found that indeed the plume persisted for more than 7 hours during these two EIS scans. From this we conclude that the blue-shift patches reflect a quasi-steady outflow pattern in the plume structure itself rather than being associated with big transient jets.

4. DISCUSSION

In the past decades, many studies have been carried out in search of the relationship between plumes and the solar wind (Walker et al. 1993; Wang 1994; Habbal et al. 1995; Hassler et al. 1999; Wilhelm et al. 2000; Giordano et al. 2000; Patsourakos & Vial 2000; Teriaca et al. 2003; Gabriel et al. 2003, 2005; McIntosh et al. 2010; Tian et al. 2011). One of the most important studies is the measurement of the outflow velocity in plume and inter-plume regions. The outflow velocity of off-limb plumes has been measured during the SOHO era (Wilhelm et al. 1998; Corti et al. 1997; Teriaca et al. 2003; Gabriel et al. 2003, 2005). However, these measurements lead to contradictory results. On the disk, Hassler et al. (1999); Hassler (2000); Wilhelm et al. (2000) measured Doppler shifts at the bright footpoints of plumes and found no obvious velocity signature since SUMER has limited spectral lines at coronal temperatures. In this study, we analysed several plumes observed by EIS on the disk. We derived their outflow velocity from hot coronal lines. In polar and low latitude regions alike, a quasi-steady outflow is present in the plumes. The outflow velocity of plumes increases with height in plumes and is found to be about 25 km s^{-1} at 0.05 $R_\odot$ above the surface. In Figure 9, we present the outflow velocity as a function of altitude measured by different authors, and insert our results shown as red crosses. This may provide further information on the velocity of the plume plasma from the solar surface out to 1.4 $R_\odot$, which should serve as an important constraint on plume models.

As mentioned in the Introduction, to estimate the possible contribution of plumes to the solar wind, we need to know the electron density to calculate the mass flux. At the height of 1.03 $R_\odot$, we also estimate the electron density by using the CHIANTI database in line pair Fe XIII 202.04 Å/Fe XIII 203.82 Å (Young et al. 2009) and obtain an electron density of 1.3×10^8 cm^{-3}. Assuming all the mass expanding from the plumes can travel to the Earth, it can contribute a proton flux of 4.2×10^9 cm^{-2}s^{-1} at 1 AU, which is an order-of-magnitude higher than that of a typical fast solar wind if a radial expansion is assumed. It should be mentioned that the plumes we analysed are mainly rooted at the boundary of CHs. The CH boundary is considered as a possible source of the slow solar wind (Wang et al. 2009; Subramanian 2010; Madjarska et al. 2012). Yet, the large mass flux that plumes can provide suggests that, plumes may be an important source of the (fast and/or slow) solar wind, but they do experience substantial lateral expansion and/or mass exchange with neighboring inter-plume plasmas.

In our study, we found that the CH regions do not show more significant blue shifts than the QS regions, which seems to contradict the consensus that CHs are the sources of the fast solar wind. The reason for this apparent contradiction is two fold. First, the radiation that EIS measured in the CHs is dominated by the stray light from the surrounding QS and active regions. Second, the solar wind may have been braked at the studied altitudes before being accelerated at higher altitudes. According to our analysis, we prefer the former interpretation. To corroborate this, we have estimated the electron density in the QS region and dark region of the CH observed on 2007 October 10, the obtained density is about 2.2×10^8 cm^{-3} and 3.7×10^8 cm^{-3} respectively. However, it is almost impossible that a CH region was denser than a typical QS region. Combined with the fact that the *RRI* parameter is almost constant in lines with high temperatures found in Section 3, this means that the radiation from the hot coronal lines is mainly from the surrounding bright area most possibly scattered by the instrument. A further study on the CH region, especially using spectroscopic observations with very low stray-light spectrometer, is needed to understand this contradiction.

5. CONCLUSION

We have measured the outflow velocity at coronal heights in several on-disk long-duration plumes observed by EIS on board Hinode, which are located in coronal holes and show significant blue shifts throughout the entire observational period. The deduced outflow velocities are quasi-steady and can reach 10 km s^{-1} at 1.02 $R_\odot$, 15 km s^{-1} at 1.03 $R_\odot$, and 25 km s^{-1} at 1.05 $R_\odot$ after corrected for the LOS effect. This clear signature of steady acceleration, combined with the fact that there is no clear blueshift at the base of plumes, provides an important constraint on plume models. At the height of 1.03 $R_\odot$, EIS also deduced a density of 1.3×10^8 cm^{-3}, resulting a proton flux of 4.2×10^9 cm^{-2}s^{-1} scaled to 1AU, which is an order of magnitude higher than necessary for the proton input to a typical solar wind if a radial expansion is assumed. This suggests that plumes may be an important source of the solar wind.

The authors would like to thank the anonymous referee for helpful comments on the manuscript. Hinode is a Japanese mission developed and launched by ISAS/JAXA, with NAOJ as domestic partner and NASA and STFC (UK) as international partners. It is operated by these agencies in co-operation with ESA and NSC

(Norway). We are grateful to Shadia Rifai Habbal for helpful discussions. This work was supported by grants NSBRSF 2012CB825601, NNSFC 41274178, 40904047, 41174154, 41274176, and the Ministry of Education of China (20110131110058 and NCET-11-0305).

REFERENCES

Ahmad, I. A., Withbroe, G. L. 1977, Sol. Phys., 53, 397
Banerjee, D., Pérez-Suárez, D., Doyle, J.G. 2009, A&A, 501, 15
Banerjee, D., Teriaca, L., Doyle, J. G., et al. 2000, Sol. Phys., 194, 43
Bělík, M., Barczyński, K., Marková, E. 2013, Sol. Phys., 284, 439
Corti, G., Poletto, G., Romoli, M., et al. 1997, ESASP, 404, 289
Cranmer, S. R., Kohl, J. L., Noci, et al. 1999, ApJ, 511, 481
Culhane, J. L., Harra, L. K., James, A. M., et al. 2007, Sol. Phys., 243, 19
Dadashi, N.; Teriaca, L.; Solanki, S. K. 2011, A&A, 534, 90
DeForest, C. E., Hoeksema, J. T., Gurman, J. B., et al. 1997, Sol. Phys., 175, 393
DeForest, C. E., Lamy, P. L., Llebaria, A. 2001, ApJ, 560, 490
DeForest, C. E.,Plunkett, S. P., Andrews, M. D. 2001, ApJ, 546, 569
Démoulin, P., Baker, D., Mandrini, C. H., et al. 2013, Sol. Phys., 283, 341
Del Zanna, G., Bromage, B. J. I., Mason, H. E. 2003, A&A, 398, 743
Del Zanna, G., Bromage, B. J. I. 1999, J. Geophys. Res., 104, 9753
Del Zanna, G., Mason, H. E. 2005, A&A, 433, 731
Feng, L., Inhester, B., Solanki, S. K., et al. 2009, ApJ, 700, 292
Gabriel, A., Bely-Dubau, F., Tison, E., et al. 2009, ApJ, 700, 551
Gabriel, A. H., Abbo, L., Bely-Dubau, F., et al. 2005, ApJ, 635, 185
Gabriel, A. H., Bely-Dubau, F., Lemaire, P. 2003, ApJ, 589, 623
Giordano, S., Antonucci, E., Noci, G.,et al .2000, ApJ, 531, 79
Gosling, J. T., Pizzo, V. J. 1999, Space Sci. Rev., 89, 21
Habbal, S. R., Esser, R., Arndt, M. B. 1993, ApJ, 413, 435
Habbal, S. R., Esser, R., Guhathakurta, M., et al. 1995, Geophys. Res. Lett., 22, 1465
Hassler, D. M. 2000, ASPC, 205, 83
Hassler, D. M., Dammasch, I. E., Lemaire, P., et al. 1999, Sci, 283, 810
Hassler, D. M., Wilhelm, K., Lemaire, P., et al. 1997, Sol. Phys., 175, 375
Kamio, S., Hara, H., Watanabe, T., et al. 2010, Sol. Phys., 266, 209
Kamio, S., Hara, H., Watanabe, T., et al. 2007, PASJ, 59, 757
Kosugi, T., Matsuzaki, K., Sakao, T., et al. 2007, Sol. Phys., 243, 3
Krieger, A. S., Timothy, A. F., Roelof, E. C. 1973, Sol. Phys., 29, 505
Madjarska, M. S., Huang, Z., Doyle, J. G., et al. 2012, A&A, 545, 67
McIntosh, S. W., Innes, D. E., de Pontieu, B., et al. 2010, A&A, 510, 2
Morgan, H., Druckmüller, M., 2014, Sol. Phys., 289, 2945
Patsourakos, S., Vial, J.-C. 2000, A&A, 359, 1
Peter, H., Judge, P. G. 1999, ApJ, 522, 1148
Rompolt, B. 1967, AcA, 17, 329
Raouafi, N.-E., Petrie, G. J. D., Norton, A. A., et al. 2008, ApJ, 682, L137
Subramanian, S., Madjarska, M. S., Doyle, J. G. 2010, A&A, 516, 50
Teriaca, L., Banerjee, D., Doyle, J. G. 1999, A&A, 349, 636
Teriaca, L., Poletto, G., Romoli, M., et al. 2003, ApJ, 588, 566
Tian, H., McIntosh, S. W., Habbal, S. R., et al. 2011, ApJ, 736, 130
Tian, H, Tu, C.-Y., Marsch, E., et al. 2010, ApJ, 709, 88
van de Hulst, H. C. 1950, BAN, 11, 135
van de Hulst, H. C. 1950, BAN, 11, 150
Velli, M., Lionello, R., Linker, J. A., et al. 2011, ApJ, 736, 32
Walker, A. B. C., Jr., Deforest, C. E., Hoover, R. B., et al. 1993, Sol. Phys., 148, 239
Wang, Y.-M., Sheeley, N. R., Jr., Dere, K. P., et al. 1997, ApJ, 484, 75
Wang, Y.-M. 1994, ApJ, 435, 153
Wang, Y.-M., Muglach, K. 2008, Sol. Phys., 29, 17
Wang, Y.-M., Sheeley, N. R., Jr. 1995, ApJ, 452, 457
Wang, Y.-M., Y.-K.Ko, R. Grappin, 1995, ApJ, 452, 457
Wilhelm, K., Abbo, L., Auchère, F., et al. 2011, A&A Rev., 19, 35
Wilhelm, K., Dammasch, I. E., Marsch, E., et al. 2000, A&A, 353, 749
Wilhelm, K., Marsch, E., Dwivedi, B. N., et al. 1998, ApJ, 500, 1023
Woo, R., 1996, ApJ, 464, 95
Xia, L. D., Marsch, E., Curdt, W. 2003, A&A, 399, 5
Xia, L. D., 2003, Geog-August-Universität Göttingen, PhD thesis
Yang, S. H., Zhang, J., Zhang, Z. Y., et al. 2011, ScChG, 54, 1906
Young, P. R., Del Zanna, G., Mason, H. E., et al. 2007, PASJ, 59, 857
Young, P. R., Watanabe, T., Hara, H., et al. 2009, A&A, 495, 587
Zirker, J. B. 1977, RvGSP, 15, 257

TABLE 1
EIS Observations Used in This Study.

Obs.ID	Scanning Period	Location	FOV(arcsec^2)	Slit	Exposure Time(s)
1	2007 Oct 10 14:03-18:16	9,889	202x512	2″	150
2	2010 Sep 04 18:30-22:02	-11,889	280x256	2″	90
3	2010 Sep 04 22:04-01:36	-11,890	280x256	2″	90
4	2011 Jan 11 09:45-13:17	-23,384	280x256	2″	90

TABLE 2
Emission Lines Used in This Study.

Line.ID	Ion	Wavelength(Å)	Log(T/K)	Region[a]	Doppler shift
1	He II	256.32	4.7	TR	No
2	Fe VIII	185.21	5.6	LC	Yes
3	Si VII	275.35	5.8	LC	Yes
4	Fe X	184.54	6.0	Cor	Yes
5	Fe XII	195.12	6.11	Cor	Yes
6	Fe XIII	202.04	6.2	Cor	Yes
7	Fe XIV	274.20	6.25	Cor	No
8	Fe XV	284.16	6.3	Cor	No

[a]TR: Transition Region; LC: Low Coronal region; Cor: Coronal region.

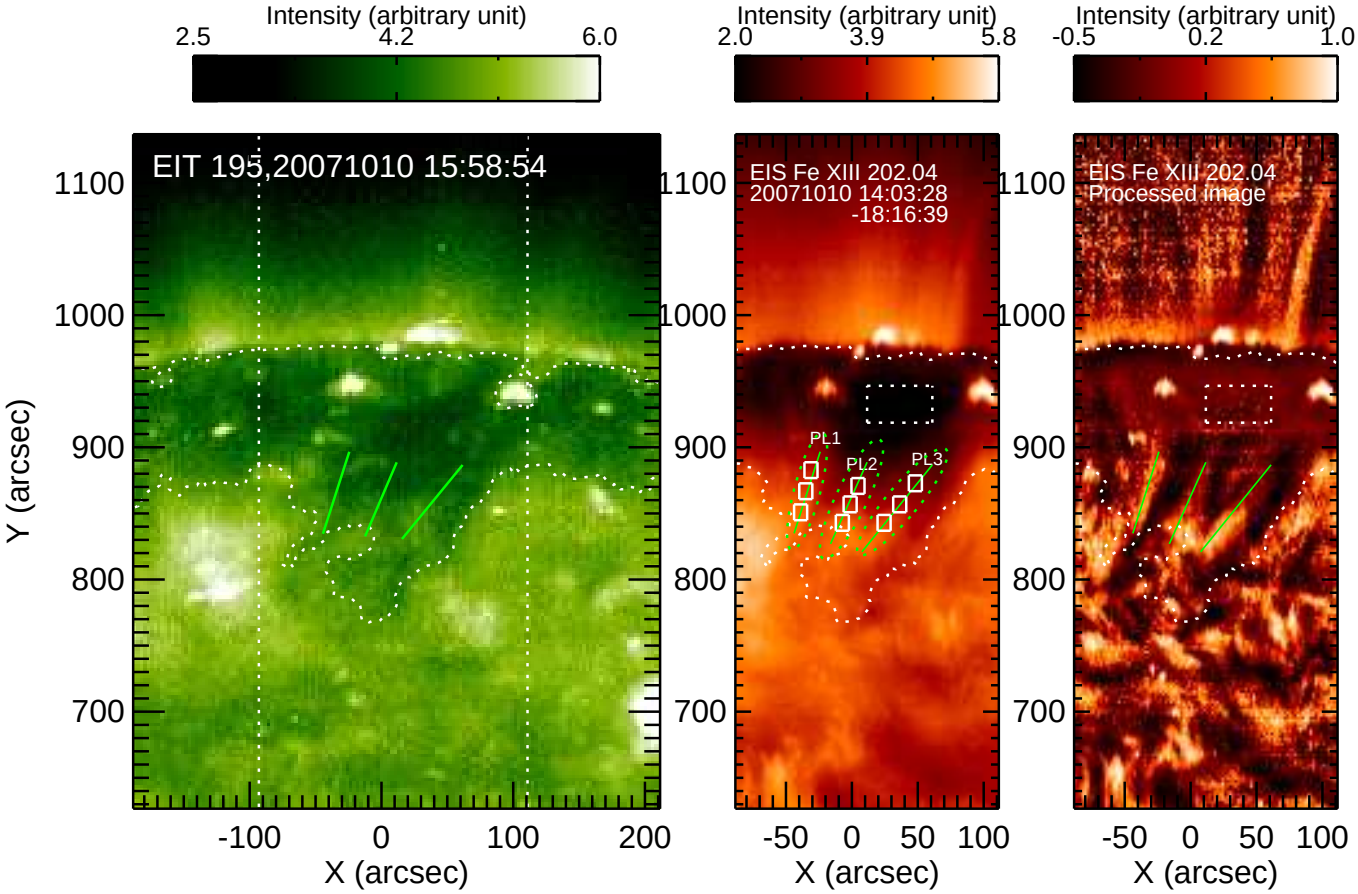

Fig. 1.— Images of the north PCH observed on 2007 October 10. The left panel shows the EIT 195 Å image with EIS field of view overplotted (vertical dotted lines). The middle panel shows the intensity map recorded by EIS in Fe XIII 202.04 Å, and the right panel shows the processed image of intensity map of EIS. The white contour lines outline the boundary of the CH, and the small region marked by the dotted line rectangle represents the typical dark region of the CH. The three tilted green full lines represent the center of the plume structures which are better seen in the processed image (right panel), and the three full line rectangles in each plume represent the plume structure from bottom to top. An EIT movie for the corresponding time interval is available online (movie20071010.mpeg).

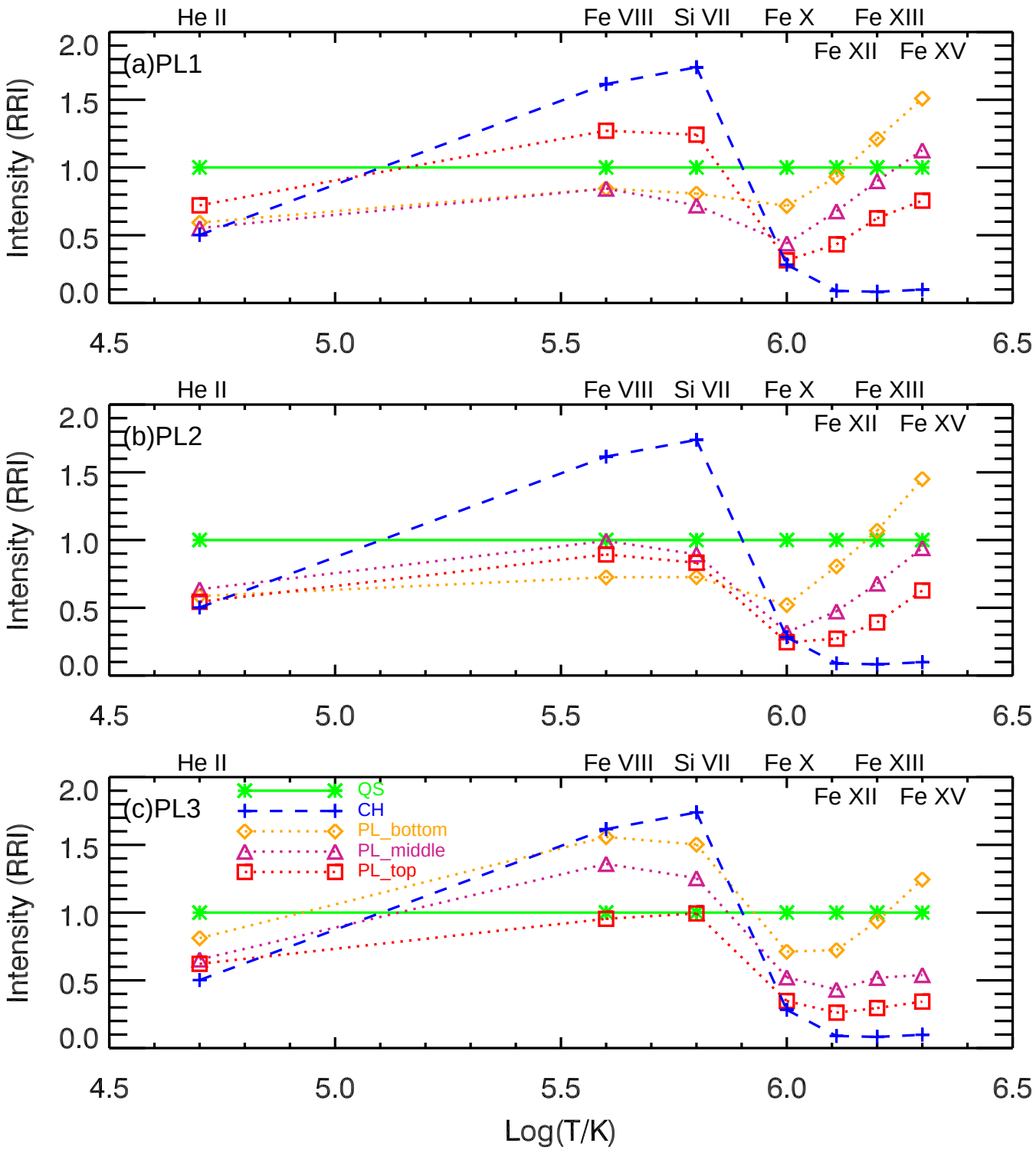

FIG. 2.— The variation of *RRI* with line formation temperature in plumes and the dark CH region. Green and blue lines represent the QS and CH regions, orange, violet red and red lines represent the plume structure from bottom to top.

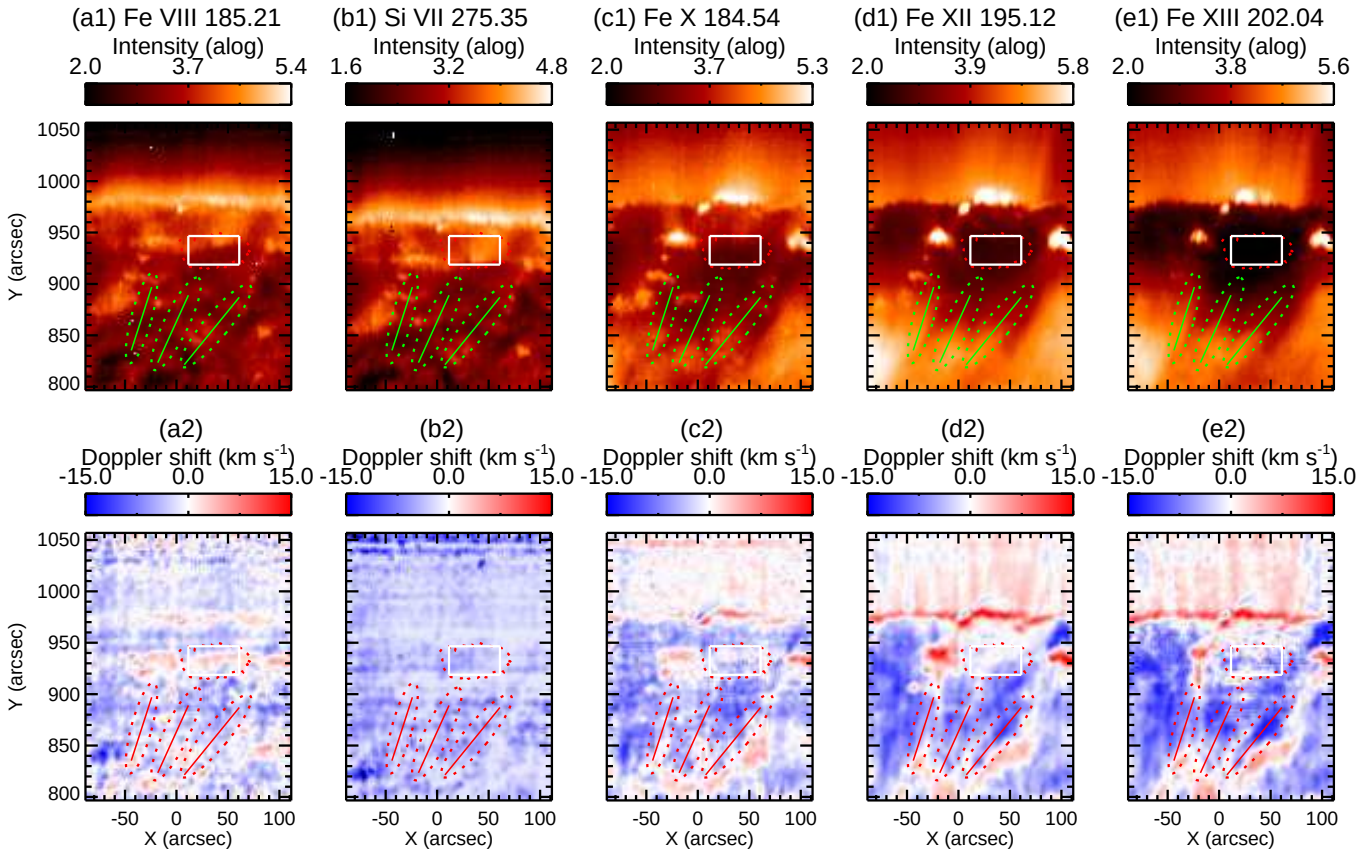

FIG. 3.— The intensity map and Dopplergram as recorded in the Fe VIII 185.21 Å, Si VII 275.35 Å, Fe X 184.54 Å, Fe XII 195.12 Å and Fe XIII 202.04 Å lines on 2007 Oct 10. The plume structures are clear in Fe XII 195.12 Å and Fe XIII 202.04 Å, and coincide with strong blue-shift patches derived from these two lines.

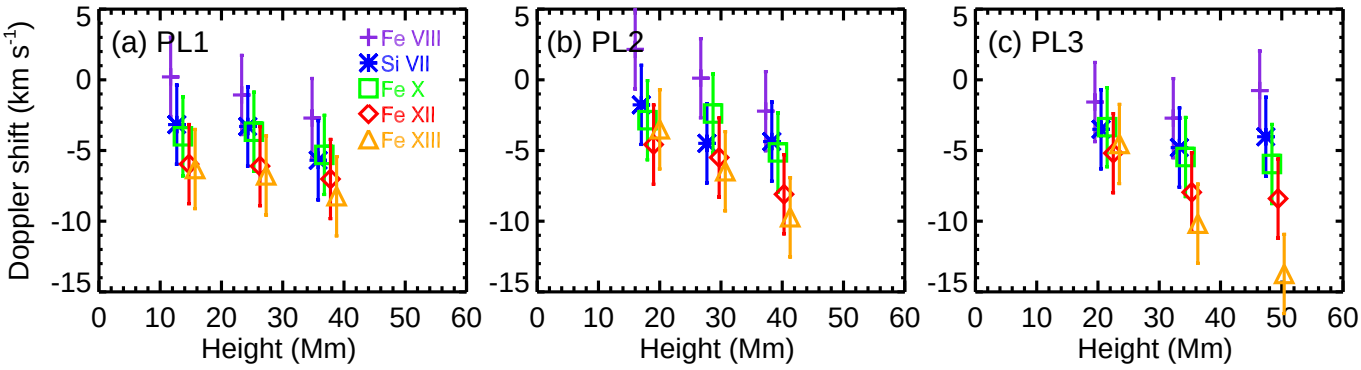

FIG. 4.— The Doppler shifts along the extended structure of plumes observed on 2007 Oct 10. For a description of how the errors are found, see text.

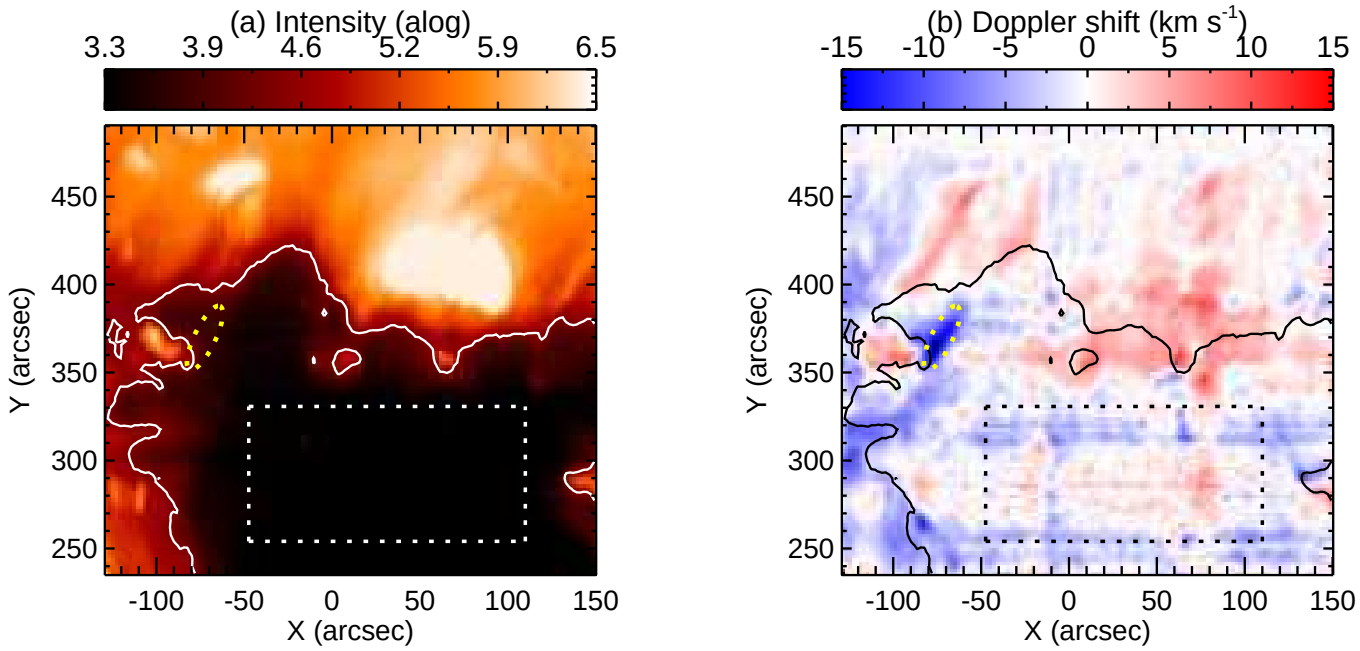

FIG. 5.— The intensity map and Dopplergram as recorded by in the Fe XII 195.12 Å line on 2011 Jan 11. The plume is outlined by yellow dotted ellipse and the rectangle represents the central part of CH. An AIA movie for the corresponding time interval is available online (movie20110111.mpeg).

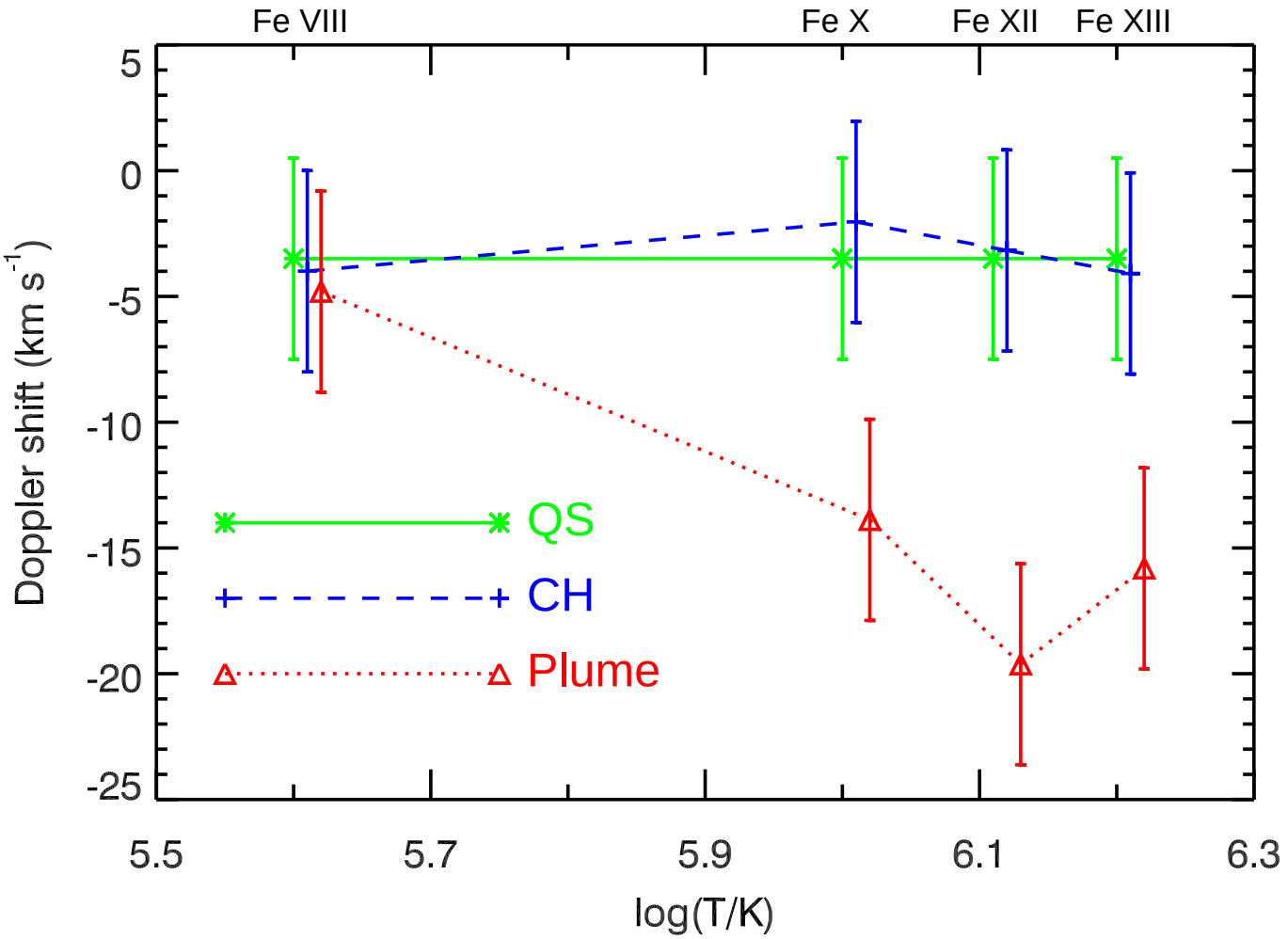

FIG. 6.— Variation of Doppler shifts with line formation temperature of the low latitude plume observed on 2011 Jan 11. Green, blue and red lines represent the QS, CH and plume region, respectively.

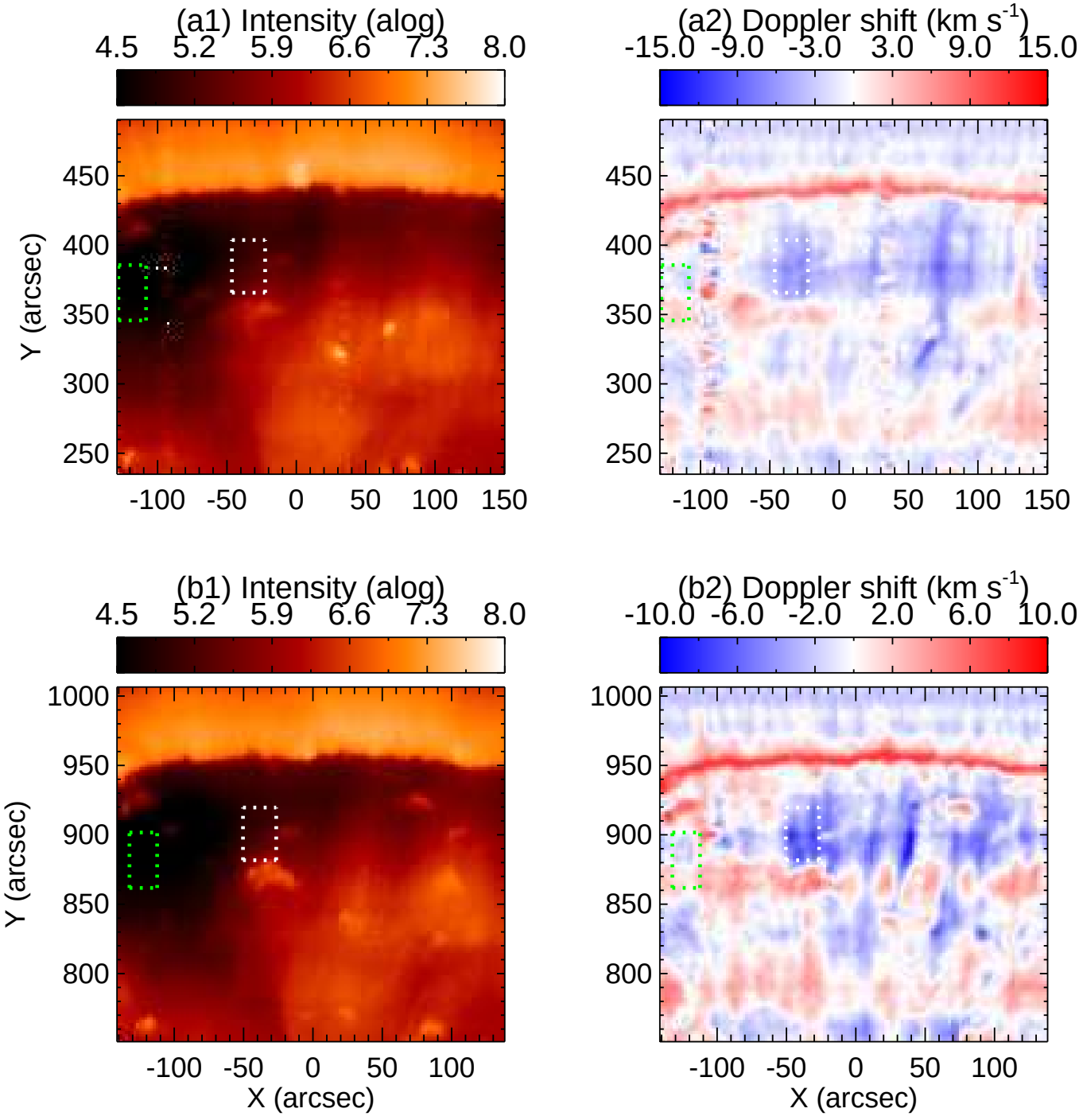

FIG. 7.— The intensity map and Dopplergram as recorded in the Fe XII 195.12 Å line on 2010 Sep 04. The top panel was observed from 18:30 to 22:02 and the bottom panel was observed from 22:04 to 01:36 the following day. The selected plume is marked by the white rectangle and the green one represents the CH region. An AIA movie for the corresponding time interval is available online (movie20100904.mpeg).

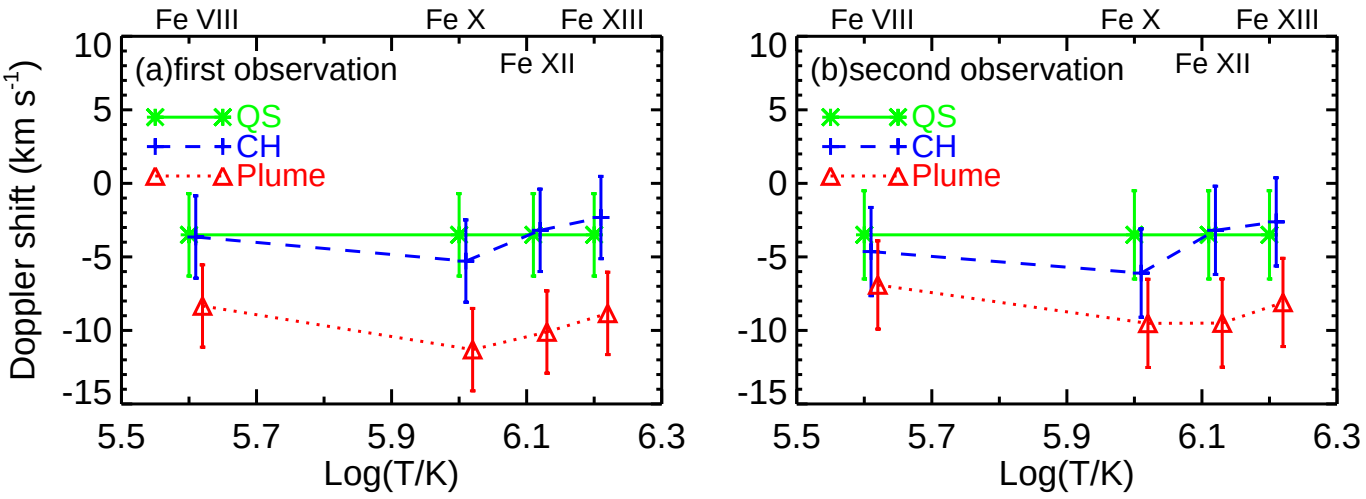

FIG. 8.— The temperature dependence of absolute Doppler shifts in a same plume observed 4 hours apart on 2010 Sep 04.

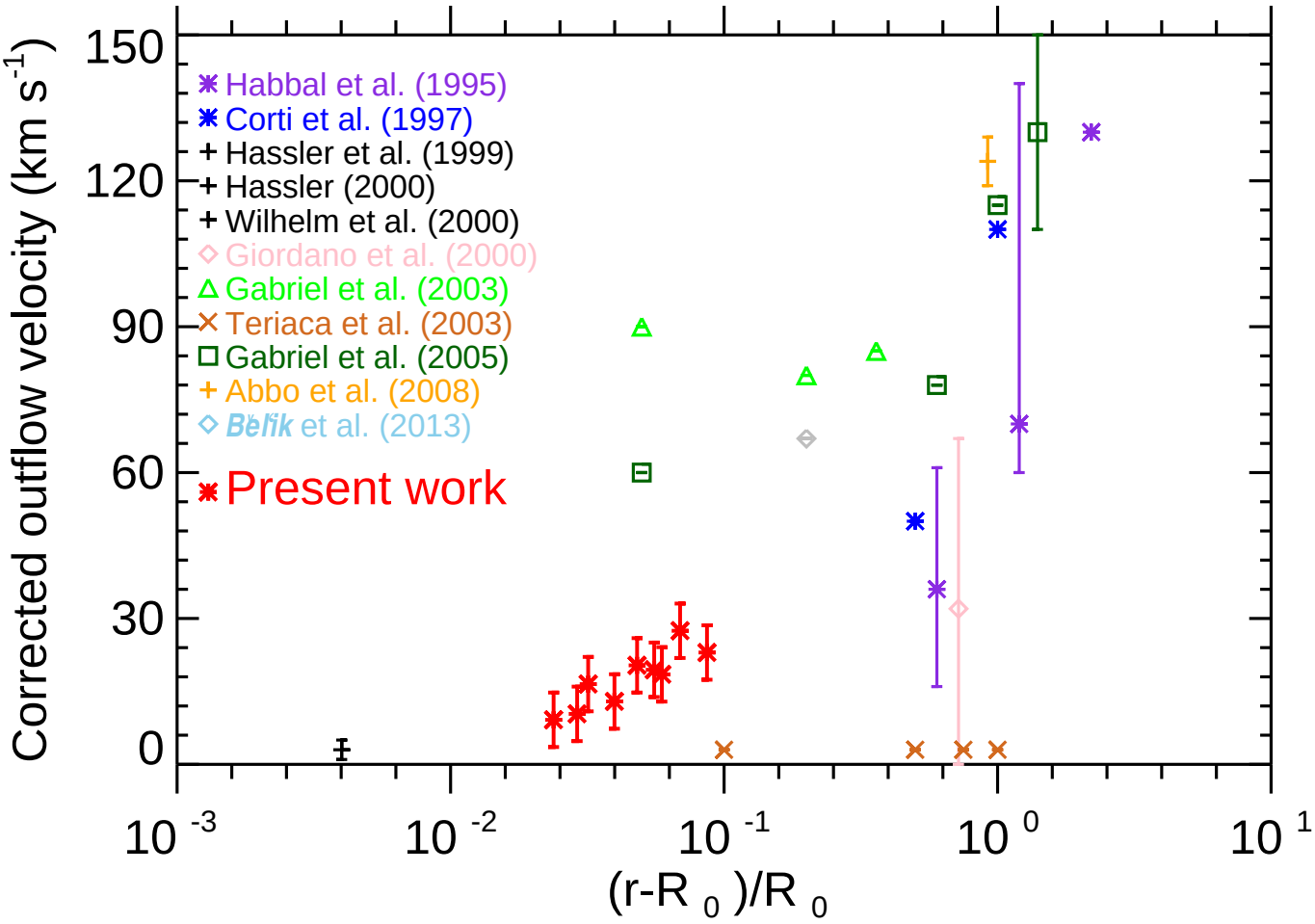

FIG. 9.— The outflow speed in plumes at different altitudes gathered from the literature. The results of the present work are shown by the red asterisk.